BIOELECTRONICS

Extracellular electrical recording of pH-triggered bursts in C6 glioma cell populations

Paulo R. F. Rocha,[1]* Maria C. R. Medeiros,[2] Ulrike Kintzel,[1] Johannes Vogt,[3] Inês M. Araújo,[4,5] Ana L. G. Mestre,[6,7] Volker Mailänder,[1,8] Paul Schlett,[1] Melanie Dröge,[1] Leonid Schneider,[1] Fabio Biscarini,[9] Dago M. de Leeuw,[1,10] Henrique L. Gomes[6,7]†

Glioma patients often suffer from epileptic seizures because of the tumor's impact on the brain physiology. Using the rat glioma cell line C6 as a model system, we performed long-term live recordings of the electrical activity of glioma populations in an ultrasensitive detection method. The transducer exploits large-area electrodes that maximize double-layer capacitance, thus increasing the sensitivity. This strategy allowed us to record glioma electrical activity. We show that although glioma cells are nonelectrogenic, they display a remarkable electrical burst activity in time. The low-frequency current noise after cell adhesion is dominated by the flow of Na^+ ions through voltage-gated ion channels. However, after an incubation period of many hours, the current noise markedly increased. This electric bursting phenomenon was not associated with apoptosis because the cells were viable and proliferative during the period of increased electric activity. We detected a rapid cell culture medium acidification accompanying this event. By using specific inhibitors, we showed that the electrical bursting activity was prompted by extracellular pH changes, which enhanced Na^+ ion flux through the psalmotoxin 1–sensitive acid-sensing ion channels. Our model of pH-triggered bursting was unambiguously supported by deliberate, external acidification of the cell culture medium. This unexpected, acidosis-driven electrical activity is likely to directly perturb, in vivo, the functionality of the healthy neuronal network in the vicinity of the tumor bulk and may contribute to seizures in glioma patients.

INTRODUCTION

All living cells maintain a membrane potential, with a negatively charged cell interior versus a positively charged cell exterior. In astrocytes, intracellular sodium concentration is kept at around 15 mM (*1*), whereas the extracellular sodium concentration ranges from 145 to 150 mM. This nonequilibrium state is mainly maintained by the Na^+- and K^+-dependent adenosine triphosphatase, which maintains intracellular sodium homeostasis by the exchange of three intracellular Na^+ ions for two extracellular K^+ ions. This then enables the buildup of a membrane potential in astrocytes with a driving force for sodium ions of about 140 mV.

Fluctuations of the membrane potential play a central role in cells of the nervous system. They are caused by the flux of primarily Na^+, K^+, Cl^-, and Ca^{2+} ions along the gradient, controlled by the function of ion channel proteins. In neurons, depolarization of the membrane potential can reach a transient reversal of electric polarity of the cell membrane, known as the action potential. Also, glia cells have long been known to express voltage-gated ion channels and to be individually electrically active (*2*). Even if glia cells cannot produce an action potential, their excitability and membrane depolarization are functionally relevant (*3*), for example, by controlling glia-mediated neurotransmitter uptake and release (*4*).

Brain tumor–derived glioma/glioblastoma cells retain many characteristics of the glia, including the expression of neurotransmitter receptors and voltage-gated ion channels (*5*). Glioma patients often suffer from epileptic seizures, which are ascribed to neurotransmitter release from the tumor cells (*6*). In healthy glia cells, this release is controlled by membrane depolarization events (*4*). Hence, it is important to understand whether, or to which extent, the same processes occur in the electrophysiology of brain tumor cells.

Extracellular activity of electrogenic cells is commonly recorded using microelectrode arrays (MEAs) with planar electrodes on a substrate in contact with cells in culture. Their main application has been the detection of action potentials in neurons. To improve the signal-to-noise ratio (SNR) and spatial resolution, filters are used to specifically detect events located at about 1 kHz. As a consequence, low-frequency events are filtered out, because their detection is impaired or even inhibited. Glia cells, as well as their transformed counterparts, glioma cells, do not exhibit action potentials. Instead, they exhibit distinctive, albeit ultraweak, single-cell oscillations of the membrane potential.

Measuring this ultraweak extracellular bioelectronic activity required us to devise a sensitive detection method based on large electrodes that exploit the large Helmholtz-Gouy-Chapman double-layer capacitance. Small extracellular voltages of cells adhered to the electrode induce a displacement current that is enhanced by a gain factor equal to the double-layer capacitance. Hence, the minute electrical activity of glia and glioma cells can be detected.

Here, we investigate the rat glioma C6 cell line as a model system for brain tumor. We recorded the electrical activity of populations of C6 cells over time; after an incubation period of a few hours, the electric current noise markedly increased. Using specific inhibitors, we showed that the electrical bursting activity is prompted by extracellular pH changes, with

[1]Max Planck Institute for Polymer Research, Ackermannweg 10, D-55128 Mainz, Germany. [2]Instituto de Telecomunicações, Departamento de Engenharia Electrotécnica e de Computadores, Universidade de Coimbra, 3030-290 Coimbra, Portugal. [3]Institute of Microanatomy and Neurobiology, University Medical Center Mainz, Langenbeckstrasse 1, 55131 Mainz, Germany. [4]Department of Biomedical Sciences and Medicine, University of Algarve, 8005-139 Faro, Portugal. [5]Centre for Biomedical Research, University of Algarve, 8005-139 Faro, Portugal. [6]Instituto de Telecomunicações, Avenida Rovisco, Pais 1, 1049-001 Lisboa, Portugal. [7]Universidade do Algarve, Faculdade de Ciências e Tecnologia, 8005-139 Faro, Portugal. [8]Dermatology Clinic, University Medicine of the Johannes-Gutenberg Universität Mainz, Langenbeckstrasse 1, 55131 Mainz, Germany. [9]Department of Life Sciences, Università di Modena e Reggio Emilia, Via Campi 103, I-41125 Modena, Italy. [10]Faculty of Aerospace Engineering, Delft University of Technology, Kluyverweg 1, 2629 HS, Delft, Netherlands.
*Present address: Department of Electronic & Electrical Engineering, University of Bath, Bath BA2 7AY, U.K.
†Corresponding author. Email: hgomes@ualg.pt

the enhancement of Na^+ ion flux through the psalmotoxin 1 (PcTX-1)–sensitive acid-sensing ion channels (ASICs). The role of pH was further confirmed by direct external acidification of the cell culture medium. Our findings hint at acid burst as an underlying mechanism contributing to epileptic events in glioma patients.

RESULTS

Detection method

A major goal of electrode fabrication for application in MEAs is to achieve low impedance because it results in a higher SNR. A target for MEAs is a ratio of 5:1 or higher. The electrodes are typically made of Au and Pt, or from alloys such as IrO_x. It is a challenge to achieve low impedance with micrometer-sized planar electrodes. Therefore, research has been focused on increasing the effective surface area by modifying the electrode with porous conducting materials, such as Pt black, Au nanostructures, carbon nanotubes, and conducting polymers. By modifying the surface, the impedance of the electrode is reduced, leading to improved electrical recordings.

Here, however, we take a different approach. We decrease the impedance by using extremely large electrode areas of a few square millimeters, orders of magnitude larger than electrode areas used in conventional MEA systems. With this approach, the noise level can be reduced to only 0.3 μVpp (microvolts peak-to-peak) (*7*). However, because of the large electrode area, individual cell signals cannot be resolved, and spatial information is lost. The measured signal is the sum of all individual cell contributions. Uncorrelated cell activity appears as noise. When the cells operate cooperatively, the signal appears as electrical spikes. Therefore, our electrode layout is optimized to pick up long–time scale synchronized signals from an entire population of cells adhered to the electrode.

The sensor comprises two circular electrodes; one of the electrodes acts as a measuring electrode, and the other one acts as a counter electrode. The equivalent circuit shown in Fig. 1A embodies the electrical coupling between the cell and the electrode. This circuit is a simplified version of the standard model used in literature (*8*, *9*). Basically, this equivalent model takes into account the electrical double layer established at a metal/electrolyte interface. The parallel circuit network is formed by the charge transfer resistance R_D and the Helmholtz-Gouy-Chapman double-layer capacitance C_D, in series with the spreading resistance R_C that accounts for the signal loss into the surrounding electrolyte. A similar circuit describes the counter electrode. The electrical path from the sensing to the counter electrode has very high impedance, Z_{seal}, because of the large distance. The cells generate a voltage, $v_s(t)$. In conventional MEAs, these voltage fluctuations are amplified by means of a voltage amplifier. Here, instead, we amplify the corresponding current fluctuations, $i_s(t)$. This current appears as a displacement current across the double-layer capacitance and is amplified by a transimpedance amplifier. The output voltage $v_o(t)$ is given by

$$v_o(t) = -R_F i_s(t) \quad (1)$$

where R_F is the feedback resistance. This detection method is referred to as the displacement current method. Details of the model can be found in a study by Medeiros *et al.* (*10*). The detected current is given as

$$i_s(t) \cong \frac{dv_S}{dt} \cdot C_D\left(1 - e^{-t/\tau}\right) \text{ with } \tau = R_C R_D \quad (2)$$

Here, τ is the time constant for the network to be charged or discharged. This equation shows that C_D is a multiplying factor, and because the area of the electrode/electrolyte interface rescales C_D by using large-area electrodes, the signal is amplified, although the spatial resolution is impaired. The current depends on the rate of change of the extracellular cell potential, and therefore, the measured signal is the derivative of the commonly measured voltage signal. Because the product $R_C C_D$ is small, the temporal resolution of the bioelectronic signals is not impaired. The displacement current measurement using large-area electrodes thus yields better sensitivity as compared to conventional voltage measurements. Furthermore, current amplification benefits from the low intrinsic electrode thermal noise at low frequencies.

As can be seen in the micrograph of Fig. 1B, cells are confluent and uniformly distributed across the entire electrode surface. The photograph was taken 10 hours after cell seeding. Details on cell growth are provided in Fig. 1C. Although cell number increases almost fivefold within 24 hours after seeding, the number of cells along the Au electrode is not expected to vary significantly during our experiments.

The entire sensing electrode is coated with a continuous monolayer of cells. From optical microscopy, we observed that each individual cell has an average area of approximately 70 μm^2. By extrapolation to the total sensing area (9.8 mm^2), we estimate that the total number of cells being probed is approximately 1.0×10^5 cells.

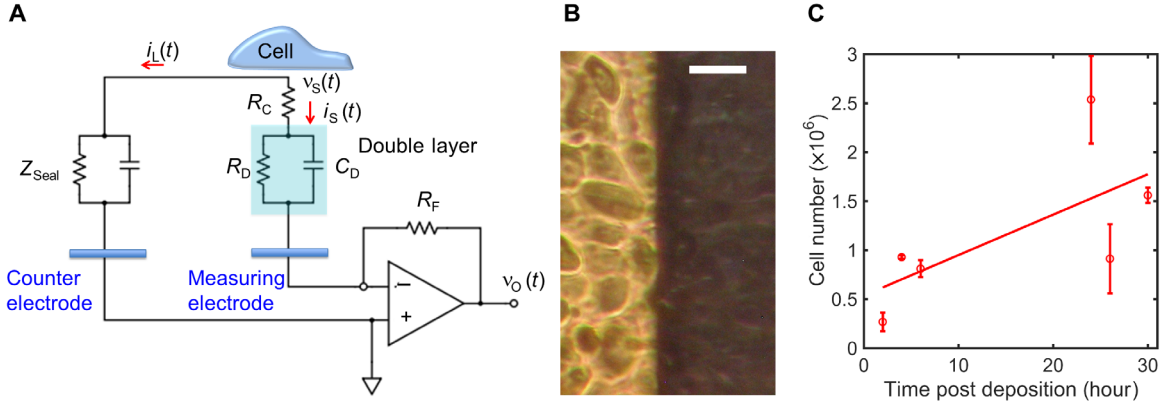

Fig. 1. Sensitive detection of C6 glioma cells. (**A**) Equivalent circuit model. (**B**) Photograph of glioma cells. The bright part denotes cells on top of the Au electrode; the darker region indicates the cells outside the Au electrode. Scale bar, 60 μm. (**C**) Cell number as a function of time after cell deposition. For all measurements, the average cell viability was 79% (±12%). Each data point was repeated five times. The straight diagonal line represents a guide to the eye.

Time evolution of electrical current noise

Freshly adhered C6 glioma cells generate a current noise on the order of 1 to 10 pA. The use of specific pharmaceutical inhibitors demonstrates that the weak current signals are dominated by the flow of Na^+ and K^+ ions through their respective voltage-gated channels (*11*).

After an incubation period of about 10 hours, the current recordings suddenly changed. A typical temporal response is presented in Fig. 2A. Here, time 0 represents the start of altered cell activity after the incubation period. This activity can be classified into three consecutive time regions with distinct spike patterns. The onset of the activity (Fig. 2A, region I) is characterized by weak sporadic spikes separated by time intervals as long as 5 min. This slow and weak activity, which is observed during the incubation period, evolves into a second pattern, region II, characterized by an increase of both the firing rate and the spikes' magnitude. Spike amplitudes rise from 10 to 80 pA, and time intervals can be as short as a few seconds. This increasing activity lasts for more than 1000 s. Following this period, activity stops for a few minutes, denoting a silent region (unlabeled). Subsequently, the spike pattern evolves into a bursting behavior, region III. Spikes appear now in clusters separated by silent regions. Both the bursts and the silent regions can be as long as 100 to 400 s. As shown in Fig. 2B, within individual bursts, spikes occasionally hint at a quasi-periodic behavior.

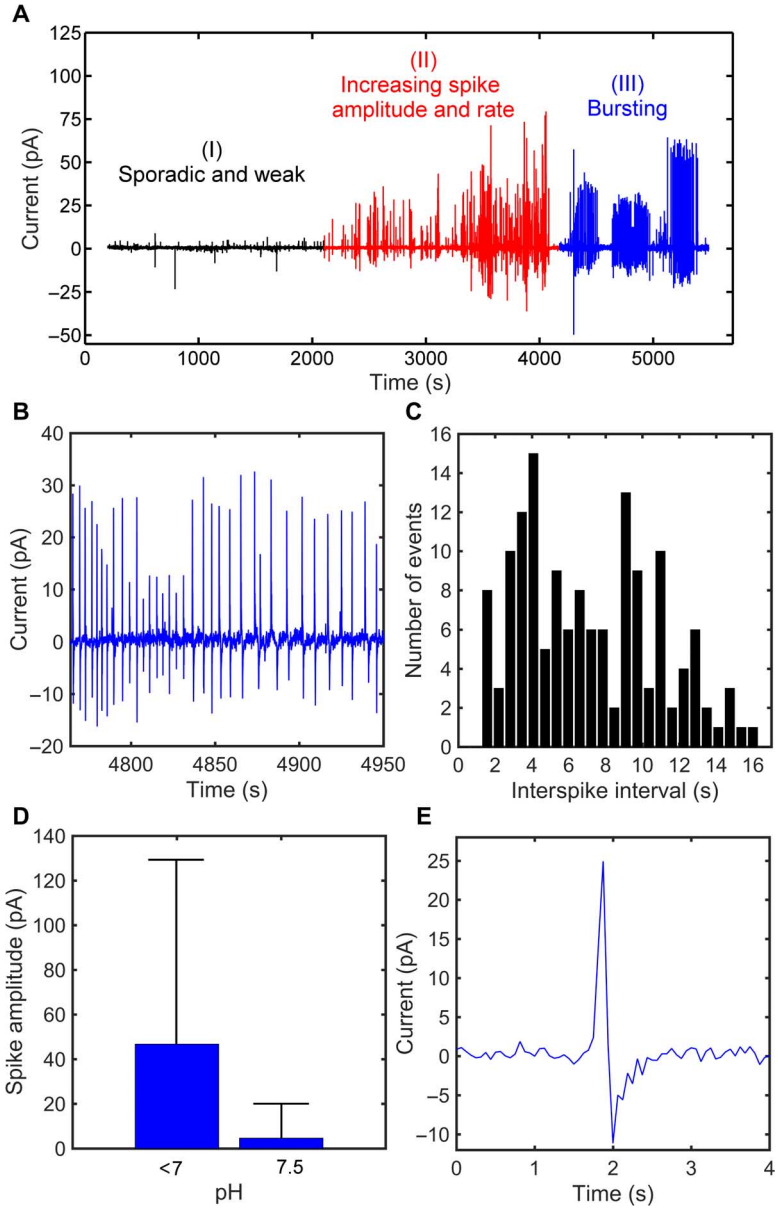

Fig. 2. Evolution of the magnitude and frequency of current noise of C6 glioma cell populations with time. (**A**) Recording of current noise with time. The recordings are taken after an incubation period of about 10 hours. Three distinct periods of activities can be detected. (**B**) Zoom-in of the current trace of the bursting activity of region III showing quasi-periodic spikes. (**C**) Histogram of the interspike intervals recorded for the whole burst activity shown in (A). The interspike intervals were distributed into time slots with a resolution of 0.36 s. (**D** and **E**) Quantitative electrical data from 10 experiments. In acidified cells, spike amplitudes ranged from 1 to 125 pA, with a mean amplitude value of 46.8 pA. In nonacidified cells, spike amplitudes varied between 1 and 20 pA, with a mean spike amplitude of 4.7 pA.

Figure 2B shows the magnified time trace of a typical bursting activity. Here, spikes are approximately equidistant, with an interspike interval between 1 and 16 s. To identify firing patterns, we analyzed the entire time bursting region of Fig. 2A and constructed the statistics of the time between two consecutive spikes. Analysis of these interspike intervals showed that the mean interspike interval (±SEM) is 9.5 ± 1 s. The skewness and kurtosis of the distribution appear significantly larger than their normal distribution thresholds, thus suggesting a non-Gaussian distribution. To evidence this, we show in Fig. 2C the histogram obtained by distributing the time intervals into 0.36-s wide bins. Time intervals shorter than 0.36 s and longer than 16 s were not considered because of their rare appearance. The histogram appears skewed to larger time intervals because of the occurrence of cooperative signaling.

Figure 2D represents the mean of 300 spike magnitudes recorded with a pH lower than 7. In all experiments, the spike magnitudes varied between 10 and 124 pA. The mean spike magnitude recorded under a pH of less than 7 is 46.8 pA. Nonacidified cells, under a pH of about 7.5, exhibit a significantly lower number of spikes. Figure 2D represents a total of 85 recorded spikes with a mean value of 4.9 pA. Spike magnitude varied between 1 and 20 pA.

Figure 2E shows a detailed view of an individual signal. Current spikes are bipolar, asymmetric, and characterized by a large positive peak with approximately twice the amplitude of the negative peak. As described above, the signal shape when measured in current is the derivative of the original voltage fluctuation at the cell/electrode interface (*10*).

The experiment was repeated more than 10 times. In 70% of all cases, an increase in noise was observed over time. The incubation time varied from a few hours to 15 hours. Occasionally, the noise evolved into bursts of low-frequency quasi-periodic spikes. We note that the measured signal is a superposition of the individual responses of all cells adhered on the electrode. Because of the arguments invoked above, we ascribe these quasi-periodic spikes to the synchronization of the signaling across the whole population on the electrode; thus, they are typical of a cooperative phenomenon.

Extracellular pH–triggered current noise

To test whether the recordings of electrical activity in C6 cultures, as shown in Fig. 2, can be traced back to apoptosis and associated membrane-depolarizing events, we performed cell growth and viability assays. As shown in Fig. 1C, cell numbers rapidly increased almost fivefold within 24 hours after seeding, whereas the average viability of the cultures remained at all points at ~79% (±12%). The cells are highly viable and proliferative when electric activity is observed. Hence, cell death can be excluded as the origin of the increase in current noise. Only after 30 hours, without medium change, does cell viability start to decrease.

Cell culture medium acidification occurred after cell seeding. The pH decrease in the culture medium could already be visually observed by the color change of the phenol red pH indicator in the cell culture medium from red to yellow. To investigate this observation, we performed kinetics studies of the pH development in the wells containing C6 cells, as opposed to cell-free medium. As shown in Fig. 3, the pH dropped about 1 U after 20 hours, and concurrently, cell population increased by 1 million cells (Fig. 1C). Our data therefore indicate a correlation between increased cell number and a drop in extracellular pH of the culture medium.

Culture medium acidification is caused by the increased metabolism of rapidly dividing cells, particularly of transformed and less contact-inhibited cells, as indeed C6 glioma cells are. Thus, we postulate that the onset of the electric bursting activity in glioma cultures is likely to be primarily caused by, or correlated with, this extracellular acidification. It is known that a decrease in the culture medium pH initiates Na^+ ion flux through (voltage-independent) ASICs on the glioma cell membrane (*12*–*14*). Glioma cells were shown to express ASICs that respond to elevated extracellular hydronium ion concentration (for example, acidified culture medium) by allowing inward Na^+ ion currents (*12*, *15*–*17*). Specifically, it has been shown that C6 glioma cells do respond to pH changes by ion currents across the cell membrane (*18*, *19*). It is therefore likely that ASICs can contribute to electric seizures in the pathogenesis of diseases associated with extracellular acidosis (*20*).

To validate the idea that electrical bursting is pH-triggered, we measured the bursting activity of C6 cells upon application of the inhibitors tetrodotoxin (TTX) and PcTX-1. TTX specifically inhibits voltage-gated Na^+ channels but does not impinge on the functionality of other types of Na^+ channels present in glioma cells (*21*, *22*). PcTX-1 is a specific inhibitor of ASICs. We first studied the effect of TTX on a population of C6 cells in a culture medium where the pH was lower than 6.8.

Figure 4 shows current noise fluctuations of an acidified C6 population of about 10 pA. External acidification causes Na^+ ion currents through ASICs, because TTX is known to block voltage-gated Na^+ channels (*21*, *22*). However, upon adding TTX up to a final concentration of 1 μM, the current noise fluctuations remain persistent. This evidence supports the hypothesis that electrical activity, being resistant to TTX, is not due to the enhanced activity of voltage-gated Na^+ channels. The enhanced activity of C6 cells upon adding TTX corresponds to the reported increased sensitivity of tumor cells in an acidic microenvironment (*23*, *24*).

To test whether the bursting is due to Na^+ ion currents through ASICs, we applied a highly specific inhibitor of ASICs (*25*), PcTX-1. The electric response exhibited spontaneous current bursting activity, as illustrated by the black curve in Fig. 5A. Right after adding PcTX-1 to the cell medium up to a concentration of 100 nM, the bursting no longer appeared, and the current fluctuations decreased to almost the background noise of our measuring system (depicted as the red curve in Fig. 5A). PcTX-1 was then removed by washing three times. Then, we waited 8 hours to let the medium acidify again. The current, represented as the blue line in Fig. 5A, shows that the original electrical behavior of glioma cells recovered.

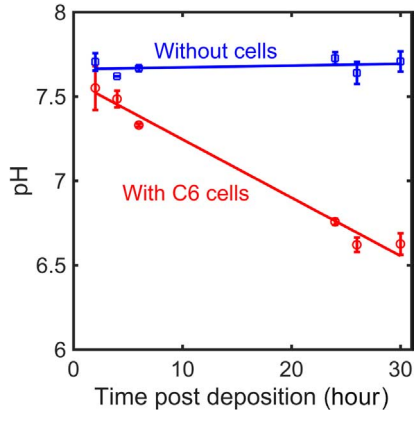

Fig. 3. pH and cell growth with time. Cell metabolism–related pH changes in culture medium. Initially, 2.3×10^5 cells were seeded in a volume of 200 μl. Each data point was repeated five times. Straight lines represent a guide to the eye.

To visualize in detail the effect of adding PcTX-1 to a population of C6 glioma cells under acidified culture conditions, we plotted the corresponding current noise spectra (S_I) in Fig. 5B. The initial S_I of the acidified C6 cells is presented in black. The typical noise spectrum follows $1/f^{\alpha}$ dependence, with $0.85 < \alpha < 2$. The noise dispersion has been attributed to stochastic variations, such as biochemical pathways, temperature variations, and opening and closing of ion channels (*26*, *27*). After adding PcTX-1, the current noise spectrum was measured again. Impressively, as little as 100 nM PcTX-1 markedly reduced current fluctuations as shown by the red line. This huge decrease in low-frequency noise could be specifically attributed to the inhibition of the ASICs. The small activity remaining was ascribed to voltage-gated Na^+ channels, as these are not affected by PcTX-1. After the cells were washed thrice and incubated for 8 hours, the noise spectrum fully recovered to that of the original state, as illustrated by the blue line in Fig. 5B. The PcTX-1 treatment efficiently reduced the electrical activity. This confirms our hypothesis that the electric bursting activity of glioma populations is prompted by extracellular pH changes, causing Na^+ ion flux through PcTX-1–sensitive channels of the ASIC family.

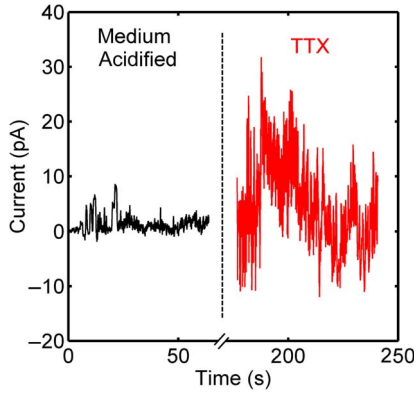

Fig. 4. Time evolution of current noise of C6 glioma cells upon adding TTX. The black trace on the left depicts the noise of acidified cells. The red trace on the right depicts the noise measured immediately after adding TTX to the acidified cell culture medium with a concentration of 1 μM.

To unambiguously assign electric bursting to extracellular pH–triggered current noise, we deliberately acidified the adhered C6 glioma cell populations. C6 glioma cells were deposited and left to adhere to the electrodes for about 10 hours. A large volume of culture medium was used to prevent extracellular acidification. The color of the medium did not change with time, and the pH measured was constant, around 7. Next, the medium was deliberately acidified with 1.0 N HCl (BioReagent, suitable for cell culture, Sigma Aldrich). The pH initially decreased to 5.9, but with time, the pH stabilized at 6.7. At this point, all the adhered cells were still viable, with viability above 95%. We note that, for in vitro glioma cell populations, similar extracellular pH values in between 6.0 and 7.5 have been reported. Normal brain tissue has a pH value of about 7.1, but the pH measured in human brain tumors has a mean value around 6.8 and can be as low as 5.9 (*28*–*30*).

The evolution of the current noise is presented in Fig. 6A. Before external acidification of the cell medium, the current noise consisted of randomly distributed fluctuations ranging from 2 to 22 pA, comparable to the sporadic and weak noise in region I of Fig. 2A. Immediately after acidification, the current noise markedly increased. Figure 6A shows that the current noise changes into a bursting activity comparable to that observed in region III in Fig. 2A. A histogram of the recorded interspike intervals is shown in Fig. 6B. The interspike distribution is skewed to larger time intervals. Because of the larger number of data points, the distribution is more pronounced than that in Fig. 2C and supports the occurrence of cooperative signaling. The bursting lasts for about 1 hour. The cells were washed, and the medium was changed. The cells were left for another 10 hours. Then, the medium was acidified again, and a similar bursting activity was measured again.

Our data demonstrate that a concerted burst activity in entire glioma cultures is correlated with the decreased extracellular pH. With their disorganized vasculature and fast growth, tumors display a strongly acidic extracellular environment due to the production of lactic acid (*31*). This strongly acidic pH is due to a metabolic shift in tumor cells toward aerobic glycolysis—even in the presence of oxygen—rather than mitochondrial oxidative phosphorylation. This occurs when too much pyruvate is present in a cell and the process of oxidative phosphorylation is at its full capacity. Thus, the excess of the pyruvate is converted

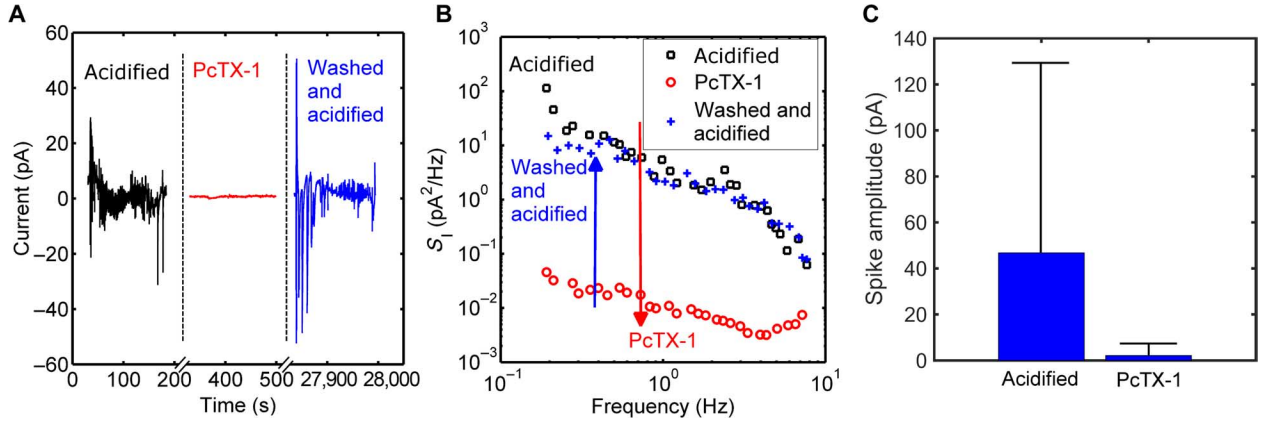

Fig. 5. Current noise of ASICs demonstrated by applying the inhibitor PcTX-1. (**A**) Time evolution of current noise of C6 glioma cells upon adding PcTX-1, up to a concentration of 100 nM in acidified cell culture medium. The black line represents the original state. The red line is recorded after adding PcTX-1 to a concentration of only 100 nM. The blue curve represents the recovery plot after thrice washing. (**B**) The corresponding current noise spectra of Fig. 4A. (**C**) The mean of 300 spike amplitudes of acidified cells as depicted in Fig. 1D. PcTX-1 data quantification recorded over two inhibitory experiments.

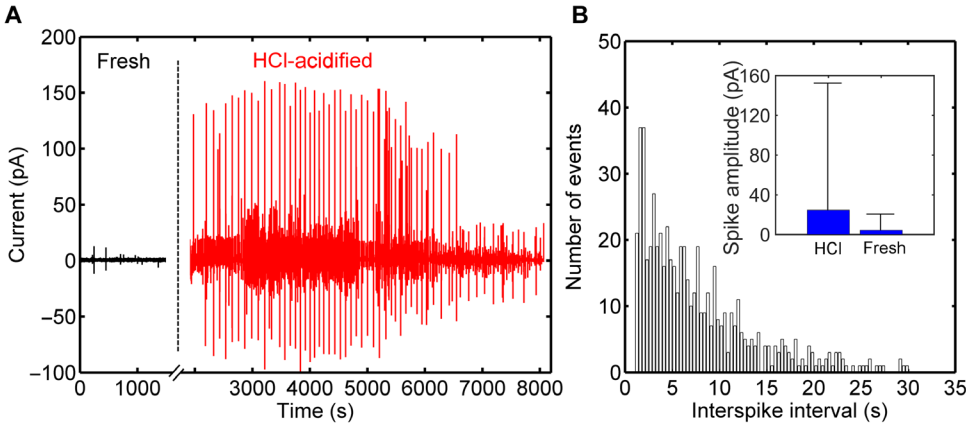

Fig. 6. External acidification of C6 glioma cells. After deposition, the cells were allowed to adhere to the electrodes for 10 hours. (**A**) The evolution of the current noise upon acidification of the medium. The current noise changes from weak and sporadic current fluctuations to a bursting activity of quasi-periodic spikes. (**B**) Histogram of the interspike intervals recorded for the entire burst activity shown in (A). The interspike intervals were distributed into time slots with a resolution of 0.36 s. Inset: Data quantification of 600 spikes comprising two distinct experiments. After the addition of HCl, the spike magnitude mean value becomes 24.7 pA. The interval recorded varies between 1 and 159.4 pA.

to lactate. This metabolic shift has been termed the "Warburg effect" and is associated with better survival and generation of substrates critically necessary in rapidly proliferating cells. However, a pH gradient, as observed in C6 gliomas in vivo (*31*), may have detrimental effects leading to synchronized cellular activity, as shown by our study.

Therefore, it would be reasonable to target the pH decrease as a potential mechanism for epileptic events in glioma patients. Clearly, the pH change in our experimental setup in a cell culture is not due to the inefficient supply of oxygen but, rather, to the exhaustion of other factors. Although the mechanism that causes the pH to drop may be different, lactate is the responsible molecule under both conditions.

The phenotypical evidence for pH-triggered electric currents in glioma cell cultures suggests that this electric activity may result in vesicular neurotransmitter release from glioma cells. Therefore, we propose further investigations to assess whether epileptic seizures may indeed be caused by the intrinsic electric activity of glioma cells and their subsequent neurotransmitter release.

DISCUSSION

We have investigated the extracellular electrical activity of rat glioma cell line C6 as a model system for brain tumor. The weak electrical activity of C6 cell populations in vitro was recorded as a function of time. The initial low-frequency current noise after cell adhesion is mainly due to the flow of Na^+ ions through voltage-gated channels. However, we found that after an incubation period of many hours, the current noise markedly increased. All electrical recordings showed bursts of current spikes of high amplitude. Occasionally, these signals also show brief quasi-periodic behavior. We demonstrate that this bursting phenomenon is not associated with apoptosis because the cells are highly viable and proliferative when the electric activity is observed. However, we detected a rapid cell culture medium acidification with time. By using specific inhibitors, we showed that the electrical bursting activity is prompted by extracellular pH change that enhances Na^+ ion flux through the PcTX-1–sensitive ASICs.

The pH-triggered bursting is unambiguously supported by experiments, which show that direct acidification of the cell culture medium led to a similar bursting behavior. This is in line with recent work showing the presence of ASICs in cultured astrocytes (*32*) and in glioma cells (*33*). However, although ASIC1 channels were found in association with epithelial sodium channels in high-grade glioma cells (such as GBM cells) (*33*), extracellular acidification (as described to be present in high-grade glioma) would result in cellular depolarization and electrical activity.

Our finding that a population of glioma cells can engage in electric activity, independent of any neuronal stimuli, may be highly relevant for understanding the tumor's impact on brain electrophysiology. In particular, the high incidence of seizures in glioma patients (*6*) and observations that gliomas directly interfere with the electrophysiology of the surrounding brain tissue (*26*) make our experimental data particularly intriguing. Future brain tumor therapies should seek to suppress this autologous electric activity of gliomas, which may account for epileptic seizures and other neurological side effects in glioma patients.

MATERIALS AND METHODS

The transducer is based on 100-nm-thick Au electrodes that are a few millimeters apart, each with an area of about 10 mm^2, evaporated on a glass substrate. A 2-nm Cr layer was used for Au adhesion. A poly (methyl methacrylate) compartment which could be filled with cells and culture medium, was glued on top of the substrate. The well was loosely covered with a lid to prevent evaporation of the medium. After filling, the system was put into an incubator (Thermo Scientific, Midi 40). This system assures the presence of enough cell culture medium to keep the cells viable over more than 24 hours without medium change.

Rat glioma C6 cells (American Type Culture Collection) were cultured in 15% F-12K nutrient mixture supplemented with 15% fetal horse serum, 2.5% fetal bovine serum, and 1% penicillin and streptomycin. The cells were maintained at 37°C in an incubator with a humidified atmosphere with 5% CO_2. The cells were harvested from the culture plates and diluted in culture medium to yield cell suspensions with a known cell density and transferred to the sensing devices. An aliquot of 350 µl of the cell suspension, with a concentration of 5.1×10^6 cells/ml, was transferred to the well of the transducer, and cells were allowed to sediment onto the electrodes for 2 hours before any measurements were performed. Before cell deposition, the transducers were sterilized by ultraviolet (UV) treatment, and the electrodes were

coated with poly-L-lysine to promote cell adhesion. UV sterilization was accomplished by using a Bio Air device with a Sankyo Denki G30T8 lamp with UV-C in the 200- to 280-nm range. Time under UV light was about 30 min. The transducer was placed 20 cm away from the lamp.

Cell viability and pH kinetics assays were performed both in the transducer and in 96-well plates. Cells (4×10^5) were seeded in 350-µl culture medium, with cell-free wells as controls. The supernatant pH was measured with a Lab 850 pH Meter (SCHOTT Instruments). Cell numbers and viability were assessed using a Neubauer chamber–based trypan blue LIVE/DEAD exclusion assay.

Cells were equally viable in the transducer and in 96-well plates. Cell number assays showed identical values for both substrates.

TTX (Sigma Ltd.) working solution (1 mg/ml) was prepared in an acetate buffer (final pH 4.4 to 4.6) according to the manufacturer's instructions. PcTX-1 (Merck Chemicals GmbH) was directly dissolved in cell culture medium (F-12K) to a working concentration of 0.1 M. Final dilutions of 1 µM TTX and 100 nM PcTX-1 were obtained by diluting the working solution in the cell culture medium. To achieve a pH decrease to 5.9, 20 µl of hydrochloric acid solution (1 N) was added to the extracellular medium. The entire experimental setup was specifically designed for ultrasensitive detection. External interference was minimized through the use of a Faraday cage and low-noise cables. To enhance the SNR, we specifically used Au electrodes, because they exhibit a large charge transfer resistance that minimizes the thermal noise. Despite the large resistance and capacitance, the R_C time constant still allows detection of low-frequency events. The experimental setup was optimized for detection below 10 Hz. Details to record the displacement current and noise analysis were published elsewhere (*10*).

The current between two Au electrodes was measured using a low-noise current amplifier (SR570, Stanford Research) and a dynamic signal analyzer (35670A, Agilent). To minimize drift, the current amplifier was calibrated and the setup was stabilized for at least 2 hours before measuring. The current was recorded as a function of time by using zero bias on the electrodes.

Any residual instrumental offset was subtracted. To visualize the small changes in current recordings, data were analyzed in the frequency domain by calculating the current noise spectrum. Reported spectra are averages over 20 consecutive recordings.

Optical micrographs showed that the C6 cells adhered and covered the whole electrode. Because of the large electrode area, the recorded current was not from a single cell, such as in MEAs, but arose from the superposition of bioelectric signals of all cells coupled to the electrode. Hence, we recorded the activity of a glioma cell population.

REFERENCES AND NOTES

1. J. W. Deitmer, C. R. Rose, Ion changes and signalling in perisynaptic glia. *Brain Res. Rev.* **63**, 113–129 (2010).
2. H. Sontheimer, Voltage-dependent ion channels in glial cells. *Glia* **11**, 156–172 (1994).
3. U. Pannasch, M. Derangeon, O. Chever, N. Rouach, Astroglial gap junctions shape neuronal network activity. *Commun. Integr. Biol.* **5**, 248–254 (2012).
4. R. Zorec, A. Araque, G. Carmignoto, P. G. Haydon, A. Verkhratsky, V. Parpura, Astroglial excitability and gliotransmission: An appraisal of Ca^{2+} as a signalling route. *ASN Neuro* **4**, 103–119 (2012).
5. T. Brismar, Physiology of transformed glial cells. *Glia* **15**, 231–243 (1995).
6. J. Pallud, L. Capelle, G. Huberfeld, Tumoral epileptogenicity: How does it happen? *Epilepsia* **54**, 30–34 (2013).
7. P. R. F. Rocha, P. Schlett, U. Kintzel, V. Mailänder, L. K. J. Vandamme, G. Zeck, H. L. Gomes, F. Biscarini, D. M. de Leeuw, Electrochemical noise and impedance of Au electrode/electrolyte interfaces enabling extracellular detection of glioma cell populations. *Sci. Rep.* **6**, 34843 (2016).
8. M. E. J. Obien, K. Deligkaris, T. Bullmann, D. J. Bakkum, U. Frey, Revealing neuronal function through microelectrode array recordings. *Front. Neurosci.* **8**, 423 (2015).
9. B. Eversmann, M. Jenkner, F. Hofmann, C. Paulus, R. Brederlow, B. Holzapfl, P. Fromherz, M. Merz, M. Brenner, M. Schreiter, R. Gabl, K. Plehnert, M. Steinhauser, G. Eckstein, D. Schmitt-Landsiedel, R. Thewes, A 128 x 128 CMOS biosensor array for extracellular recording of neural activity. *IEEE J. Solid-State Circuits* **38**, 2306–2317 (2003).
10. M. C. R. Medeiros, A. Mestre, P. Inácio, S. Asgarif, I. M. Araújo, P. C. Hubbard, Z. Velez, M. L. Cancela, P. R. F. Rocha, D. M. de Leeuw, F. Biscarini, H. L. Gomes, An electrical method to measure low-frequency collective and synchronized cell activity using extracellular electrodes. *Sens. Bio-Sensing Res.* **10**, 1–8 (2016).
11. P. R. F. Rocha, P. Schlett, L. Schneider, M. Dröge, V. Mailänder, H. L. Gomes, P. W. M. Blom, D. M. de Leeuw, Low frequency electric current noise in glioma cell populations. *J. Mater. Chem. B* **3**, 5035–5039 (2015).
12. N. Kapoor, R. Bartoszewski, Y. J. Qadri, Z. Bebok, J. K. Bubien, C. M. Fuller, D. J. Benos, Knockdown of ASIC1 and epithelial sodium channel subunits inhibits glioblastoma whole cell current and cell migration. *J. Biol. Chem.* **284**, 24526–24541 (2009).
13. B. K. Berdiev, J. Xia, L. A. McLean, J. M. Markert, G. Y. Gillespie, T. B. Mapstone, A. P. Naren, B. Jovov, J. K. Bubien, H.-L. Ji, C. M. Fuller, K. L. Kirk, D. J. Benos, Acid-sensing ion channels in malignant gliomas. *J. Biol. Chem.* **278**, 15023–15034 (2003).
14. R. Waldmann, G. Champigny, F. Bassilana, C. Heurteaux, M. Lazdunski, A proton-gated cation channel involved in acid-sensing. *Nature* **386**, 173–177 (1997).
15. A. K. Rooj, C. M. McNicholas, R. Bartoszewski, Z. Bebok, D. J. Benos, C. M. Fuller, Glioma-specific cation conductance regulates migration and cell cycle progression. *J. Biol. Chem.* **287**, 4053–4065 (2012).
16. W. H. Vila-Carriles, G. G. Kovacs, B. Jovov, Z.-H. Zhou, A. K. Pahwa, G. Colby, O. Esimai, G. Y. Gillespie, T. B. Mapstone, J. M. Markert, C. M. Fuller, J. K. Bubien, D. J. Benos, Surface expression of ASIC2 inhibits the amiloride-sensitive current and migration of glioma cells. *J. Biol. Chem.* **281**, 19220–19232 (2006).
17. A. Honasoge, H. Sontheimer, Involvement of tumor acidification in brain cancer pathophysiology. *Front. Physiol.* **4**, 316 (2013).
18. M. Erecińska, D. Nelson, F. Dagani, J. Deas, I. A. Silver, Relations between intracellular ions and energy metabolism under acidotic conditions: A study with nigericin in synaptosomes, neurons, and C6 glioma cells. *J. Neurochem.* **61**, 1356–1368 (1993).
19. K. Glunde, H. Düßmann, H.-P. Juretschke, D. Leibfritz, Na^+/H^+ exchange subtype 1 inhibition during extracellular acidification and hypoxia in glioma cells. *J. Neurochem.* **80**, 36–44 (2002).
20. J. A. Wemmie, C. C. Askwith, E. Lamani, M. D. Cassell, J. H. Freeman, M. J. Welsh, Acid-sensing ion channel 1 is localized in brain regions with high synaptic density and contributes to fear conditioning. *J. Neurosci.* **23**, 5496–5502 (2003).
21. C. H. Lee, P. C. Ruben, Interaction between voltage-gated sodium channels and the neurotoxin, tetrodotoxin. *Channels* **2**, 407–412 (2008).
22. A. Tamura, N. Yamada, Y. Yaguchi, Y. Machida, I. Mori, M. Osanai, Both neurons and astrocytes exhibited tetrodotoxin-resistant metabotropic glutamate receptor-dependent spontaneous slow Ca^{2+} oscillations in striatum. *PLOS ONE* **9**, e85351 (2014).
23. O. Tredan, C. M. Galmarini, K. Patel, I. F. Tannock, Drug resistance and the solid tumor microenvironment. *J. Natl. Cancer Inst.* **99**, 1441–1454 (2007).
24. S. Simon, D. Roy, M. Schindler, Intracellular pH and the control of multidrug resistance. *Proc. Natl. Acad. Sci. U.S.A.* **91**, 1128–1132 (1994).
25. P. Escoubas, J. R. De Weille, A. Lecoq, S. Diochot, R. Waldmann, G. Champigny, D. Moinier, A. Ménez, M. Lazdunski, Isolation of a tarantula toxin specific for a class of proton-gated Na^+ channels. *J. Biol. Chem.* **275**, 25116–25121 (2000).
26. D. A. Mathers, J. L. Barker, Spontaneous voltage and current fluctuations in tissue cultured mouse dorsal root ganglion cells. *Brain Res.* **293**, 35–47 (1984).
27. E. Sejdić, L. A. Lipsitz, Necessity of noise in physiology and medicine. *Comput. Methods Programs Biomed.* **111**, 459–470 (2013).
28. P. Vaupel, F. Kallinowski, P. Okunieff, Blood flow, oxygen and nutrient supply, and metabolic microenvironment of human tumors: A review. *Cancer Res.* **49**, 6449–6465 (1989).
29. F. Kallinowski, P. Vaupel, pH distributions in spontaneous and isotransplanted rat tumours. *Br. J. Cancer* **58**, 314–321 (1988).
30. J. Chiche, M. C. Brahimi-Horn, J. Pouysségur, Tumour hypoxia induces a metabolic shift causing acidosis: A common feature in cancer. *J. Cell. Mol. Med.* **14**, 771–794 (2010).
31. P. Swietach, A. Hulikova, R. D. Vaughan-Jones, A. L. Harris, New insights into the physiological role of carbonic anhydrase IX in tumour pH regulation. *Oncogene* **29**, 6509–6521 (2010).
32. C. Huang, Z.-l. Hu, W.-N. Wu, D.-F. Yu, Q.-J. Xiong, J.-R. Song, Q. Shu, H. Fu, F. Wang, J.-G. Chen, Existence and distinction of acid-evoked currents in rat astrocytes. *Glia* **58**, 1415–1424 (2010).
33. N. Kapoor, W. Lee, E. Clark, R. Bartoszewski, C. M. McNicholas, C. B. Latham, Z. Bebok, V. Parpura, C. M. Fuller, C. A. Palmer, D. J. Benos, Interaction of ASIC1 and ENaC subunits in human glioma cells and rat astrocytes. *Am. J. Physiol. Cell Physiol.* **300**, C1246–C1259 (2011).

Acknowledgments

Funding: We acknowledge support from the European Commission, Seventh Framework Programme (FP7; 2007–2013), through project iONE FP7, grant agreement 280772, and from the Portuguese Foundation for Science and Technology (FCT), through the project Intelligent Cell Surfaces EuroBioSAS/0001/2010, PEst-OE/EEI/LA0008/2013, and the project Implantable Organic Devices for Advanced Therapies (INNOVATE) PTDC/EEI-AUT/5442/2014. **Author contributions:** M.C.R.M., P.R.F.R., and H.L.G. conceived the concept and analyzed the detection method. M.C.R.M. also suggested the importance of acidification. U.K. and M.D. performed pH and cell viability measurements and C6 cell handling. J.V., V.M., and I.M.A. supervised the biological part of the project. P.R.F.R., M.C.R.M., and A.L.G.M. performed electrical measurements. P.S. automated the recordings and wrote the software for the data analysis. L.S. suggested and demonstrated with PcTX-1 the role of ASICs. M.C.R.M., P.R.F.R., J.V., H.L.G, D.M.d.L., F.B. and L.S. wrote the manuscript. D.M.d.L. and H.L.G. supervised the project.

Competing interests: The authors declare that they have no competing interests. **Data and materials availability:** All data needed to evaluate the conclusions in the paper are present in the paper. Additional data related to this paper may be requested from the authors.

Submitted 10 March 2016
Accepted 18 November 2016
Published 23 December 2016
10.1126/sciadv.1600516

Citation: P. R. F. Rocha, M. C. R. Medeiros, U. Kintzel, J. Vogt, I. M. Araújo, A. L. G. Mestre, V. Mailänder, P. Schlett, M. Dröge, L. Schneider, F. Biscarini, D. M. de Leeuw, H. L. Gomes, Extracellular electrical recording of pH-triggered bursts in C6 glioma cell populations. *Sci. Adv.* **2**, e1600516 (2016).

ScienceAdvances

Extracellular electrical recording of pH-triggered bursts in C6 glioma cell populations

Paulo R. F. Rocha, Maria C. R. Medeiros, Ulrike Kintzel, Johannes Vogt, Inês M. Araújo, Ana L. G. Mestre, Volker Mailänder, Paul Schlett, Melanie Dröge, Leonid Schneider, Fabio Biscarini, Dago M. de Leeuw, and Henrique L. Gomes

Sci. Adv., **2** (12), e1600516.
DOI: 10.1126/sciadv.1600516